Progress In Electromagnetics Research, PIER 16, 175–203, 1997

MULTISCALE SURFACE ROUGHNESS AND BACKSCATTERING

A.T. Manninen*

Finnish Institute of Marine Research
P.O. Box 33
FIN-00931, Helsinki, Finland

1. INTRODUCTION

Surface roughness is usually described with the two classical constant parameters, rms height and correlation length, which is determined using the autocorrelation function. Unfortunately, the rms height and correlation length of natural surfaces, such as sea ice, depend on the measured distance [1,2]. This is understandable since the shape of natural solid surfaces is often a result of a number of random changes superposed on an initial surface. Spectral analysis would permit multiscale roughness, but the spectrum of a sparse data set does not represent the real target spectrum well. A description for a surface with multiscale roughness was developed using autocorrelation functions and is presented in this paper.

* Present address: VTT Automation, Remote Sensing, P.O.Box 13031, FIN-02044, VTT, Finland. Email: Terhikki.Manninen@vtt.fi.

The recent development of the Integral Equation Method for calculating surface backscattering coefficients has removed the limitation of older surface backscattering models, that the surface roughness should be either small or large compared to the wavelength used [3–5,7]. However, even this method is usually applied assuming that the surface roughness can be described with the two classical constant parameters, rms height and correlation length. The problem of surfaces having both small and large scale roughness characteristics has been studied in several cases [1,3,6,8], but the use of the IEM equations for calculating the surface backscattering coefficients for surfaces having multiscale roughness requires further consideration. This problem is also studied in this paper for cases having small dielectric constant values, such as sea ice [3].

2. SURFACE CORRELATION FOR A CONTINUOUS ROUGHNESS SPECTRUM

Natural surfaces are typically results of a sequence of random changes affecting an initial surface. Such surfaces can be treated in the same way as multilayer stacks [8]. The initial surface is described with a profile $z_1(x)$. A random process $h_2(x)$ then changes the surface profile with an additive roughness so that the new surface profile is $z_2(x) = z_1(x) + h_2(x)$. The additive roughness can also be negative so that the superposition produces a smoother surface than the original. It is natural to assume that the initial and final surfaces are partially correlated. As more changes take place, more additive components appear and the final surface profile is [8]

$$z_n(x) = z_1(x) + \sum_{i=2}^{n} h_i(x) \tag{1}$$

The final surface correlation function is then obtained as a sum of the original surface correlation and the autocorrelation of the random changes [8]. Conventional finish analysis uses a sum of exponentials and Gaussians to describe the final surface autocorrelation function [1]

$$\rho(\xi) = \sum_i \sigma_i^2 \exp(-|\xi|/L_i) + \sum_j \sigma_j^2 \exp(-(\xi/L_j)^2) \tag{2}$$

where σ_i is the rms height and L_i the correlation length of the ith roughness component.

When a surface undergoes changes perpetually due to changing weather conditions (like a sea ice surface), it is natural to replace the summations of Eq. 2 with an integral. Likewise the resulting roughness spectrum is considered to contain a continuous range of spatial frequencies instead of only discrete values.

The estimation of surface correlation parameters is always affected by the inner and outer scales [9], which give the limits for the minimum and maximum spatial frequencies possible to detect using a certain measurement trace length. Thus, the verification of the continuous roughness spectrum is not trivial. The autocorrelation function and the power spectrum of a surface carry the same information since they are a Fourier transform pair, but the power spectrum is less sensitive to the finite measurement trace length of a profile [1]. However, the power spectrum of a data set does not approach the real target spectrum when the number of points in the profile increases [10]. Only the expectation value of the spectrum approaches the true target value. The spectrum is also very sensitive to individual grooves or peaks in a profile [Fig. 1]. Moreover in practice the number of measured heights is often rather small, which makes the use of the power spectrum even more unreliable. In addition, the surface backscattering coefficient can not be obtained analytically for a general power spectrum. The existing analytical methods for calculating the surface backscattering coefficient for dielectric materials are developed using the autocorrelation function. Therefore an attempt has been made in this paper to develop an autocorrelation function that takes into account multiscale surface roughness.

In practice, it is impossible to measure all the random changes that have affected the surface. The only possible roughness to be measured is the final result, but one would also need measured values of all the intermediate surfaces to apply Eq. 2 directly. A practical solution is to measure the final surface using various measurement trace lengths from small to large distances so that various final roughness scales are characterized. Since it is not possible to detect the largest roughness components from the smallest distances, it can be thought that the smallest measurement trace lengths give results that would be obtained, if the largest roughness components of Eq. 2 were missing. In addition, the roughness parameters corresponding to a certain distance are dominated by the largest roughness scale that is distinguishable with that measurement trace length. Thus, it is reasonable

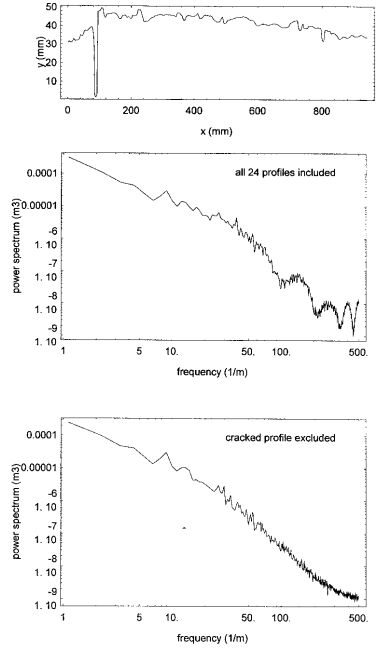

Figure 1. The surface profile of a Baltic sea ice sample having a crack. The spectrum of the ensemble of profiles measured in the same area is shown when the ensemble includes the profile with a crack and when it excludes it.

to think that the roughness components of the summation in Eq. 2 can be estimated with the roughness components obtained from the final surface using various measurement trace lengths.

For natural surfaces the rms height and the correlation length typically depend on the measured length [1,2]. When the dependence is assumed to be of the same form for all roughness components from small to large distances the rms height and correlation length of increasing intervals x_i can be described with the following equations

$$\sigma_i = f(x_i), \quad i = 1, \cdots, n \tag{3}$$

$$\rho(\xi, \zeta)_i = g(\xi, \zeta; x_i), \quad i = 1, \cdots, n \tag{4}$$

where f and g denote arbitrary functions. Generalizing the result to a continuously increasing distance with a maximum value x_o, we get an

equation corresponding to Eq. 2

$$\rho(\xi,\zeta) = \int_0^{x_o} \frac{f(x)^2}{f_o} \cdot g(\xi,\zeta;x)dx \tag{5}$$

where $f_o = \int_0^{x_o} f(x)^2 dx$ so that the value of the correlation function at zero is unity.

If the form of the dependence of rms height and correlation length on distance is not the same in the whole interval of interest, one can divide the interval into sections where the form is invariant and then combine these sections as in the two-scale roughness case.

The behaviour of natural surfaces is often close to that of Brownian surfaces. Then the correlation length L is linearly dependent on the measurement length x [1]

$$L = k_o x \tag{6}$$

where k_o is a constant. Also, the logarithm of the rms height σ is usually linearly dependent on the logarithm of x, so that [2]

$$\sigma = c \cdot x^b \tag{7}$$

where c is a constant.

Commonly used surface correlation functions are Gaussian, exponential, isotropic exponential and transformed exponential given by equations [3]

$$\rho(\xi,\zeta) = \exp[-(\xi^2+\zeta^2)/L^2] \tag{8}$$

$$\rho(\xi,\zeta) = \exp[-(|\xi|+|\zeta|)/L] \tag{9}$$

$$\rho(\xi,\zeta) = \exp\left[-\sqrt{(\xi^2+\zeta^2)/L^2}\right] \tag{10}$$

$$\rho(\xi,\zeta) = 1/[1+(\xi^2+\zeta^2)/L^2]^{\frac{3}{2}} \tag{11}$$

respectively.

The corresponding surface correlation functions corresponding to multiscale roughness described by Eqs. 6 and 7 are now according to Eqs. 3–11 [11,12]

$$\rho(\xi,\zeta) = \frac{1}{2}(1+2b)\left(\frac{\xi^2+\zeta^2}{k_o^2 x_o^2}\right)^{1/2+b}\Gamma\left(-\frac{1}{2}-b, \frac{\xi^2+\zeta^2}{k_o^2 x_o^2}\right) \tag{12}$$

$$\rho(\xi,\zeta) = (1+2b)\left(\frac{|\xi|+|\zeta|}{k_o x_o}\right)^{1+2b}\Gamma\left(-1-2b, \frac{|\xi|+|\zeta|}{k_o x_o}\right) \tag{13}$$

$$\rho(\xi,\zeta) = (1+2b)\left(\frac{\sqrt{\xi^2+\zeta^2}}{k_o x_o}\right)^{1+2b}\Gamma\left(-1-2b, \frac{\sqrt{\xi^2+\zeta^2}}{k_o x_o}\right) \tag{14}$$

$$\rho(\xi,\zeta) = \frac{(1+2b)}{2(2+b)}\left(\frac{\xi^2+\zeta^2}{k_o^2 x_o^2}\right)^{-3/2}{}_2F_1\left(\frac{3}{2}, 2+b; 3+b; -\frac{k_o^2 x_o^2}{\xi^2+\zeta^2}\right) \tag{15}$$

for Gaussian, exponential, isotropic exponential and transformed exponential type of surface correlation respectively. Here Γ denotes the incomplete gamma function and ${}_2F_1$ the hypergeometric function. The rms height σ for the whole surface, is obtained from the rms height σ_o, corresponding to the maximum distance x_o, using the following relationship

$$\sigma = \sigma_o/\sqrt{2b+1} \tag{16}$$

The surface correlation functions representing surfaces of single scale roughness and multiscale roughness are shown in Figure 2 for exponential, transformed exponential and Gaussian cases of equal correlation lengths. The shapes of the multiscale curves require that they be calculated using a longer distance than that of the single scale case to obtain an equally large correlation length (Fig. 3). This is understandable, since the inclusion of smaller roughness scales naturally decreases correlation. Still, the net effect of the inclusion of the smaller roughness scales is slightly destructive at short distances, whereas the correlation falls off more slowly with increasing distance than in the case of the one roughness scale.

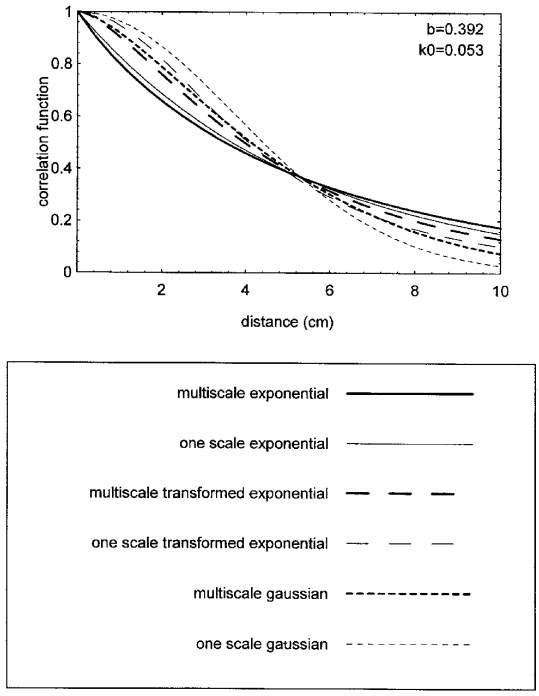

Figure 2. The surface correlation functions corresponding to Eqs. 8–11 (one scale surface roughness) and Eqs. 12–15 (continuous surface roughness spectrum) calculated for a measured slightly deformed Baltic sea ice surface. The maximum distance used in the calculations is 1 m to correspond to the measured autocorrelation function curve, which was closest to the multiscale exponential case.

If the surface in question contains only separate frequency bands, Eq. 5 can be replaced by the following equation

$$\rho(\xi,\varsigma) = \sum_{i=1}^{n} \int_{0}^{x_{max_i}} \frac{f(x)^2}{f_o} \cdot g(\xi,\varsigma;x)dx - \sum_{i=1}^{n} \int_{0}^{x_{min_i}} \frac{f(x)^2}{f_o} \cdot g(\xi,\varsigma;x)dx \tag{17}$$

where x_{max_i} is the maximum distance and x_{min_i} the minimum

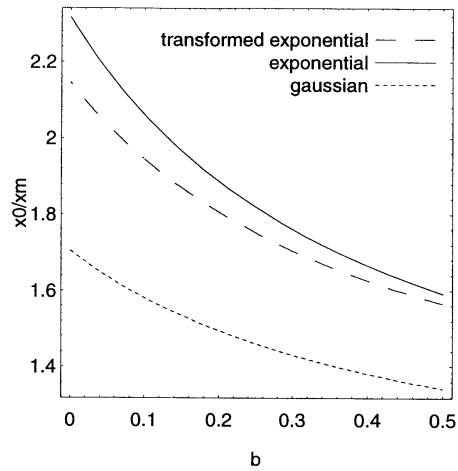

Figure 3. The ratio of the maximum distance x_o to be used in mulstiscale calculations and the measurement distance x_m that produces the same correlation length value, is shown for various values of parameter b of Eq. 7 and various types of isotropic surface correlation.

distance taken into account in band i and

$$f_o = \sum_{i=1}^{n} \int_0^{x_{max_i}} f(x)^2 dx - \sum_{i=1}^{n} \int_0^{x_{min_i}} f(x)^2 dx \tag{18}$$

so that the correlation function at zero distance is still unity. Then the surface correlation functions corresponding to Eqs. 12–15 are

$$\begin{aligned} \rho(\xi,\zeta) = & \frac{(1+2b)}{2\sum_{j=1}^{n}\left(x_{max_j}^{1+2b} - x_{min_j}^{1+2b}\right)} \sum_{i=1}^{n} \left[\left(\frac{\xi^2+\zeta^2}{k_o^2 x_{max_i}^2} \right)^{1/2+b} \right. \\ & \cdot \Gamma\left(-\frac{1}{2} - b, \frac{\xi^2+\zeta^2}{k_o^2 x_{max_i}^2} \right) x_{max_i}^{1+2b} - \left(\frac{\xi^2+\zeta^2}{k_o^2 x_{min_i}^2} \right)^{1/2+b} \\ & \left. \cdot \Gamma\left(-\frac{1}{2} - b, \frac{\xi^2+\zeta^2}{k_o^2 x_{min_i}^2} \right) x_{min_i}^{1+2b} \right] \end{aligned} \tag{19}$$

$$\rho(\xi,\zeta) = \frac{(1+2b)}{\sum_{j=1}^{n} x_{max_j}^{1+2b} - x_{min_j}^{1+2b}} \sum_{i=1}^{n} \left[\left(\frac{|\xi|+|\zeta|}{k_o x_{max_i}} \right)^{1+2b} \cdot\Gamma\left(-1-2b, \frac{|\xi|+|\zeta|}{k_o x_{max_i}}\right) x_{max_i}^{1+2b} - \left(\frac{|\xi|+|\zeta|}{k_o x_{min_i}} \right)^{1+2b} \Gamma\left(-1-2b, \frac{|\xi|+|\zeta|}{k_o x_{min_i}}\right) x_{min_i}^{1+2b} \right] \tag{20}$$

$$\rho(\xi,\zeta) = \frac{(1+2b)}{\sum_{j=1}^{n} x_{max_j}^{1+2b} - x_{min_j}^{1+2b}} \sum_{i=1}^{n} \left[\left(\frac{\sqrt{\xi^2+\zeta^2}}{k_o x_{max_i}} \right)^{1+2b} \cdot\Gamma\left(-1-2b, \frac{\sqrt{\xi^2+\zeta^2}}{k_o x_{max_i}}\right) x_{max_i}^{1+2b} - \left(\frac{\sqrt{\xi^2+\zeta^2}}{k_o x_{min_i}} \right)^{1+2b} \cdot\Gamma\left(-1-2b, \frac{\sqrt{\xi^2+\zeta^2}}{k_o x_{min_i}}\right) x_{min_i}^{1+2b} \right] \tag{21}$$

$$\rho(\xi,\zeta) = \frac{(1+2b)}{2(2+b)\left(\sum_{j=1}^{n} x_{max_j}^{1+2b} - x_{min_j}^{1+2b}\right)} \sum_{i=1}^{n} \left[\left(\frac{\xi^2+\zeta^2}{k_o^2 x_{max_i}^2} \right)^{\frac{-3}{2}} \cdot{}_2F_1\left(\frac{3}{2}, 2+b; 3+b; -\frac{k_o^2 x_{max_i}^2}{\xi^2+\zeta^2}\right) x_{max_i}^{1+2b} - \left(\frac{\xi^2+\zeta^2}{k_o^2 x_{min_i}^2} \right)^{\frac{-3}{2}} \cdot{}_2F_1\left(\frac{3}{2}, 2+b; 3+b; -\frac{k_o^2 x_{min_i}^2}{\xi^2+\zeta^2}\right) x_{min_i}^{1+2b} \right] \tag{22}$$

The shape of the autocorrelation curves obtained using Eqs. 19–22 is between those of the multiscale and single scale roughness cases. If the surface in question is characterized by different autocorrelation types in different scales, the total autocorrelation function can naturally be obtained as a combination of two or more of Eqs. 19–22 so that the values of x_{max_i} and x_{min_i} used in each equation correspond to the relevant scales.

3. CALCULATION OF THE SURFACE BACKSCATTERING COEFFICIENT

The surface backscattering coefficient derived using the integral equation method (IEM) is given by [3 - 5, 13]

$$\sigma_{pp}^0 = \frac{k^2}{2}\exp(-2k_z^2\sigma^2)\sum_{n=1}^{\infty}\left|I_{pp}^n\right|^2\frac{W^{(n)}(-2k_x,0)}{n!} \tag{23}$$

where k is the wave number, σ is the rms height, $k_z = k\cos\theta$, $k_x = k\sin\theta$, $pp = vv \;\; or \;\; hh$, θ is the incidence angle,

$$\begin{aligned} I_{pp}^n = {} & (2k_z\sigma)^n f_{pp}\exp(-k_z^2\sigma^2) \\ & + \frac{(k_z\sigma)^n\left[F_{pp}(-k_x,0) + F_{pp}(k_x,0)\right]}{2} \end{aligned} \tag{24}$$

and the spectrum for the correlation function to the nth power is

$$W^{(n)}(u,v) = \frac{1}{2\pi}\int_{-\infty}^{\infty}\int_{-\infty}^{\infty}\rho(\xi,\zeta)^n\exp(-ju\xi - jv\zeta)d\xi d\zeta,$$

$$n = 1, 2, \cdots \tag{25}$$

Other symbols are given in Appendix 2A of [3]. Actually Eq. 25 contains the surface shape description although the rms height appears in other parts of the surface backscattering coefficient formula. The dielectric constant is involved only in the field coefficients. Typically one of these is significantly larger than the other two. Then the dielectric behaviour and the surface properties of the target affect the scattering separately.

For backscattering $u = 2k_o\sin\theta$ and $v = 0$. Moreover, the correlations of Eqs. 12–15 are symmetrical with respect to origin. Thus, the imaginary part of Eq. 25 is cancelled out and it suffices to integrate only the following equation

$$W^{(n)}(u,0) = \frac{4}{2\pi}\int_0^{\infty}\int_0^{\infty}\rho(\xi,\zeta)^n\cos(u\xi)d\xi d\zeta, \quad n = 1, 2, \cdots \tag{26}$$

This integral can not be solved analytically for the four cases of Eqs. 12–15. Direct numerical integration using standard methods is not

possible either, since the integrand can be highly oscillating depending on the value of u. However, the integral can be simplified with a change of variables. Hence, the integrals to be solved numerically are

$$W^{(n)}(u,0) = \frac{2}{\pi}k_o^2 x_o^2 \int_0^\infty \left[\frac{1}{2}(1+2b)x^{1+2b}\Gamma\left(-\frac{1}{2}-b, x^2\right)\right]^n \cdot \left(\int_0^1 \cos(uk_o x_o x t)\sqrt{1-t^2}x dt\right) dx \tag{27}$$

$$W^{(n)}(u,0) = \frac{2}{\pi}k_o^2 x_o^2 \int_0^\infty [(1+2b)x^{(1+2b)}\Gamma(-1-2b,x)]^n \cdot \left(\int_0^x \cos(uk_o x_o z)dz\right) dx \tag{28}$$

$$W^{(n)}(u,0) = \frac{2}{\pi}k_o^2 x_o^2 \int_0^\infty [(1+2b)x^{(1+2b)}\Gamma(-1-2b,x)]^n \cdot \left(\int_o^1 \cos(uk_o x_o x t)\sqrt{1-t^2}x dt\right) dx \tag{29}$$

$$W^{(n)}(u,0) = \frac{2}{\pi}k_o^2 x_o^2 \int_0^\infty \left[\frac{(1+2b)}{2(2+b)}x^{-3}{}_2F_1\left(\frac{3}{2}, 2+b; 3+b; -\frac{1}{x^2}\right)\right]^n \cdot \left(\int_0^1 \cos(uk_o x_o x t)\sqrt{1-t^2}x dt\right) dx \tag{30}$$

for Gaussian, exponential, isotropic exponential and transformed exponential type of surface correlation respectively, for a continuous roughness spectrum. These four expressions can then be integrated analytically for one variable, the result being

$$W^{(n)}(u,0) = \frac{k_o x_o}{u}\int_0^\infty \left[\frac{1}{2}(1+2b)x^{1+2b}\Gamma\left(-\frac{1}{2}-b, x^2\right)\right]^n \cdot (J_1(uk_o x_o x))dx \tag{31}$$

$$W^{(n)}(u,0) = \frac{2}{\pi}\frac{k_o x_o}{u}\int_0^\infty [(1+2b)x^{1+2b}\Gamma(-1-2b,x)]^n \sin(uk_o x_o x)dx \tag{32}$$

$$W^{(n)}(u,0) = \frac{k_o x_o}{u}\int_0^\infty [(1+2b)x^{1+2b}\Gamma(-1-2b,x)]^n J_1(uk_o x_o x)dx \tag{33}$$

$$W^{(n)}(u,0) = \frac{k_o x_o}{u}\int_0^\infty \left[\frac{(1+2b)}{2(2+b)}x^{-3}{}_2F_1\left(\frac{3}{2},2+b;3+b;-\frac{1}{x^2}\right)\right]^n \cdot(J_1(uk_o x_o x))dx \tag{34}$$

Still, the oscillating behaviour of the integrand does not always permit direct conventional numerical integration. The use of Euler's method [14] turned out to be successful in the numerical integration of Eqs. 31–34. This method is based on a summation of differences of integrals between some ten first consecutive zeros. This summation converges more quickly than the direct sum of the alternating series of integral values between the consecutive zeros.

Calculation of the surface backscattering coefficients using IEM also requires the determination of the Kirchhoff coefficient f_{qp} and the complementary field coefficients F_{qp}, which depend on the Fresnel reflection coefficients $R_\perp$ and $R_\parallel$. When the dielectric constant value is small, these coefficients depend strongly on the value of the local angle. In IEM equations the local angle has been approximated with the incidence angle. Another alternative is usually a zero value for the local angle [3]. Experimental measurements of Baltic sea ice show that in practice, the variation of the local angle may cause considerable change in the values of f_{qp} and F_{qp} as will be shown in the next section [15]. However, the effect of surface parameter variation on backscattering of one target material can be studied using only relative values of σ^o. Then the field coefficient terms often have only a negligible effect in practice.

4. APPLICATION TO BALTIC SEA ICE

In order to measure those properties of Baltic sea ice that are relevant for SAR imagery interpretation research, the Finnish Institute of Ma-

rine Research arranged field experiments in two ERS-1 Pilot Projects in 1992 (PIPOR = A Programme for International Polar Oceans Research), 1993 and 1994 (OSIC = Operational sea ice charting using ERS-1 SAR images). Extensive measurements of small and medium scale surface roughness in the Bay of Bothnia revealed a clear relationship between the rms height and the correlation length of sea ice [15]. Moreover, the correlation length turned out to be linearly dependent on the measured distance. Similarly, the logarithm of the rms height showed a linear dependence on the logarithm of the measured distance. The surface correlation function was mostly close to exponential. This applied reasonably well also to ridged areas, although they do not constitute a continuous surface. This is very practical, since now deformed areas and level ice can be treated similarly when calculating the backscattering.

Examples of multiscale surface roughness of Baltic sea ice are shown in Figures 4–7. The spectra have been calculated as ensemble averages of individual measured surface profile spectra and the autocorrelation functions as ensemble averages of individual measured surface profile autocorrelation functions [15,1]. All these profiles have been measured in three areas of about 100 m $\times$ 100 m, except a few small scale profiles in Figure 6, which were situated about 100 m from the rest of the data. Figure 5 represents a many times deformed old ice field in the Bay of Bothnia in 1993 [15]. The data of Figure 6 was gathered in a huge newly formed net-like rubbled area in the Sea of Bothnia in 1994 [15]. Figure 7 corresponds to a very smooth old level ice field that was situated in the Gulf of Finland in 1994 [15]. The spectra of all the three studied ice surfaces are closer to those of fractal than conventional surfaces in the whole studied range [1]. The multiscale autocorrelation functions of Eqs. 12–15 do not have analytical Fourier transforms, but numerical studies showed that these autocorrelation functions produce power spectra resembling those of Fig. 4.

In order to compare how well one and multiscale autocorrelation functions approximate the experimental curve, the deviation area between the experimental curve and the approximative functions from origin to correlation length has been calculated. The smaller the ratio of the multiscale area to the one scale area is, the superior the multiscale autocorrelation function is. This deviation area ratio varies from 0.48 to 2.14 for the exponential surface correlation cases of Figs. 5–7. When the multiscale surface correlation of the small scale case of

Fig. 7 is changed into transformed exponential surface correlation, the deviation area ratio of multiscale and one scale functions varies from 0.42 to 0.98. Thus, the shape of a multiscale autocorrelation function gives in every case a better alternative than an ordinary one scale function for the studied small, medium and large scale cases. However, it is much more important that the multiscale parameters b and k_0 (Eqs. 6 and 7) obtained from the medium and large scale measurements produce reasonable autocorrelation functions for the small scale cases (Figs. 5–7). The slight difference is probably partly caused bythe small number of profiles in the ensembles and also by the different measurement techniques. The small scale profiles were continuous 1 m long curves digitized with an increment of 1 mm, but the medium scale profiles consisted of 100 discrete points with an increment of 5 cm and the large scale profiles of 100 discrete points with an increment of 50 cm. The multiscale autocorrelation curves proved to be successful also for other studied large scale sea ice types, because they decrease more steeply close to the origin than the corresponding single scale exponential curves.

The small scale curves are not quite as clearly exponential as those of medium or large scale, because some of the individual profiles were closer to a Gaussian or transformed exponential type. Yet only the very smooth level ice is better described with a multiscale transformed exponential than the ordinary exponential surface correlation. However, the rounding of the autocorrelation function at the origin can also be an artifact caused by the finite profile length [1]. The stylus wheel diameter used in the small scale measurements was 1 cm, which also artificially increased the closest correlations.

The Integral Equation Method for calculating surface backscattering can be applied to a wide scale of surface roughness, if the surface is random Gaussian and stationary. For Baltic sea ice these two conditions seem to be justified. This method can be used for cases smaller than the wavelength, comparable to it and larger than it.

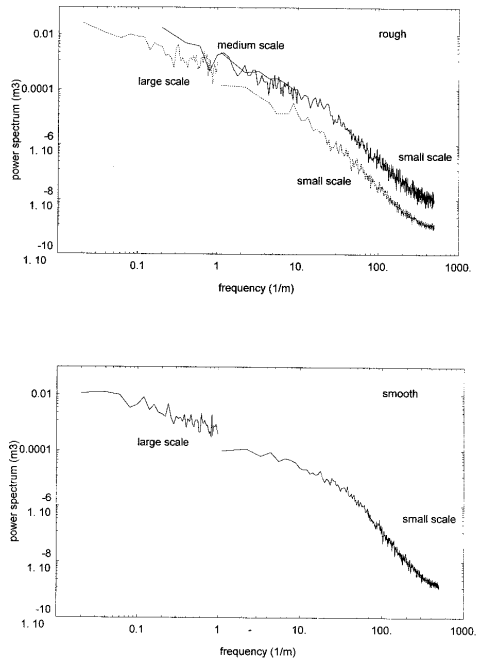

Figure 4. The spectra of measured large, medium, and small scale profiles of rough and smooth Baltic sea ice. The solid curves of rough sea ice represent a many times deformed old ice field in the Bay of Bothnia in 1993 [15, 16]. The medium scale experimental curve is an ensemble average of seven 5 m long individual profiles. The small scale experimental curve is an ensemble average of 24 individual 0.9 m long profiles. The dashed curves of rough sea ice represent a net-like rubbled newly formed ice field in the Sea of Bothnia in 1994 [15, 16]. The large scale experimental curve is an ensemble average of four 50 m long individual profiles. The small scale experimental curve is an ensemble average of 17 individual 0.9 m long profiles. The smooth sea ice curves represent an old level ice field in the Gulf of Finland in 1994 [15]. The large scale experimental curve is an ensemble average of six 50 m long individual profiles. The small scale experimental curve is an ensemble average of 18 individual 0.9 m long profiles. The number of profiles included in the small scale ensembles is smaller than was measured, to include only profiles of equal length.

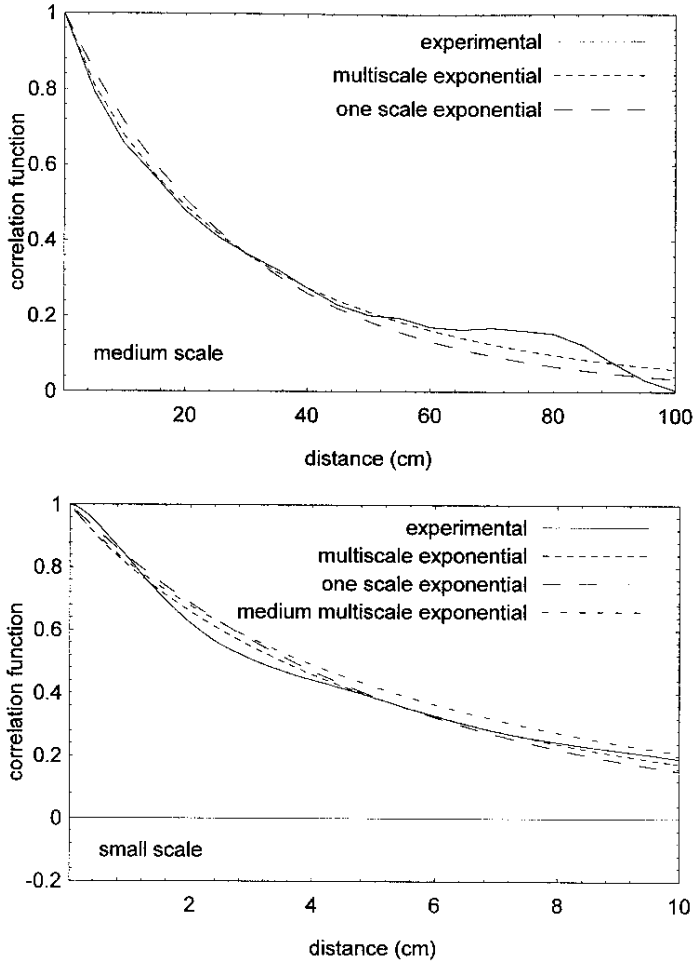

Figure 5. The measured and calculated medium and small scale autocorrelation functions of a many times deformed old ice field in the Bay of Bothnia in 1993 [15,16]. The medium scale experimental curve is an ensemble average of seven 5 m long individual profiles. The small scale experimental curve is an ensemble average of 24 individual 1 m long profiles. The multiscale autocorrelation function calculated for the 1 m distance, using the medium scale values for b and k_0 is also shown for comparaison.

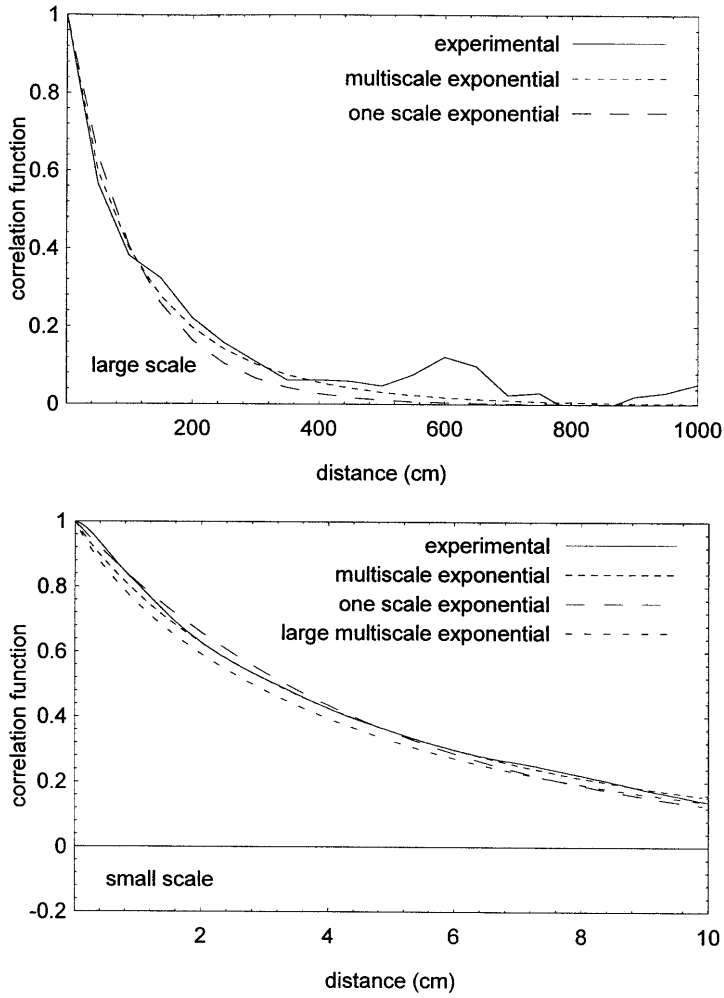

Figure 6. The measured and calculated large and small scale autocorrelation functions of a net-like rubbled newly formed ice field in the Sea of Bothnia in 1994 [15,16]. The large scale experimental curve is an ensemble average of four 50 m long individual profiles. The small scale experimental curve is an ensemble average of 24 individual 1 m long profiles. The multiscale autocorrelation function calculated for the 1 m distance, using the large scale values for b and k_0, is also shown for comparison.

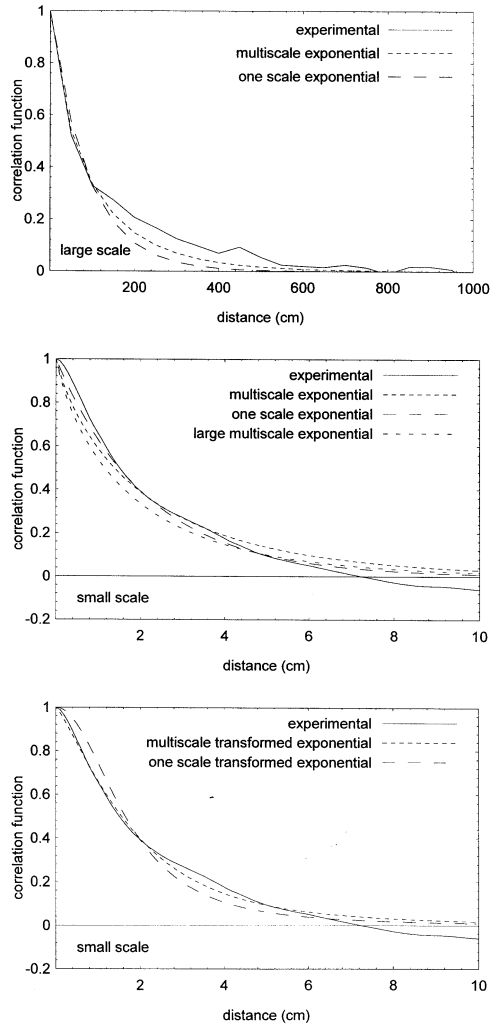

Figure 7. The measured and calculated large and small scale autocorrelation functions of a very smooth old level ice field in the Gulf of Finland in 1994 [15]. The large scale experimental curve is an ensemble average of six 50 m long individual profiles. The small scale experimental curve is an ensemble average of 24 individual 1 m long profiles. The multiscale autocorrelation function calculated for the 1 m distance, using the large scale values for b and k_0, is also shown for comparison.

The problem of using the Integral Equation Method of one scale surface roughness for sea ice is clarified in Figure 8. The backscattering coefficient was calculated using measured surface roughness parameter values corresponding to various lengths within the small and medium scale profiles. Since the rms height and correlation length increase with measurement trace length, the backscattering constant varies also with distance. Moreover, the surface roughness parameters do not generally saturate within a few metres. In some cases they do not saturate even within 100 m [15]. It is difficult to decide, which backscattering coefficient value of Figure 8 (or a value larger than these) one should choose for simulating the backscattering caused by the ERS-1 SAR, whose wavelength is about 5.7 cm and pixel size roughly 25 m. Even the ensemble average would not solve the problem of a backscattering coefficient that continuously increases with the size of the area included in the calculation. In principle the whole illuminated area should be taken into account, but usually it is thought that the roughness scale close to the wavelength used is the most important. However, there is no rule on how to choose the exact roughness value to be used.

Since the application of IEM taking into account only one roughness scale is problematic, it is useful to check how the inclusion of all roughness scales changes the situation. Figures 9 and 10 show the difference between the backscattering coefficients calculated using the ordinary IEM equations [3] and the multiscale IEM based on Eq. 33. The deformed ice field of Figure 9 is an example, where the multiscale surface roughness has a destructive effect on the backscattering even in large distances, whereas the multiscale roughness increases the backscattering for most of the ice types in Figure 10. Basically, the backscattering coefficient varies with increasing distance the same way as in Figure 9. Only the intensity level and the steepness of the curve vary.

Clearly the inclusion of all roughness scales has a slightly destructive effect on the surface autocorrelation function for all studied autocorrelation types (Fig. 2). The net effect on the backscattering coefficient is also negative for the smallest distances, because of the shape of the oscillating integral of Eqs. 31–34. However, the multiscale backscattering increases more strongly with increasing distance than that of the ordinary IEM and surpasses the one scale backscattering for many ice types already in an area having a diameter of about 50 m (Fig. 10). These results have been obtained using the isotropic exponential surface correlation and the comparison has been made using for

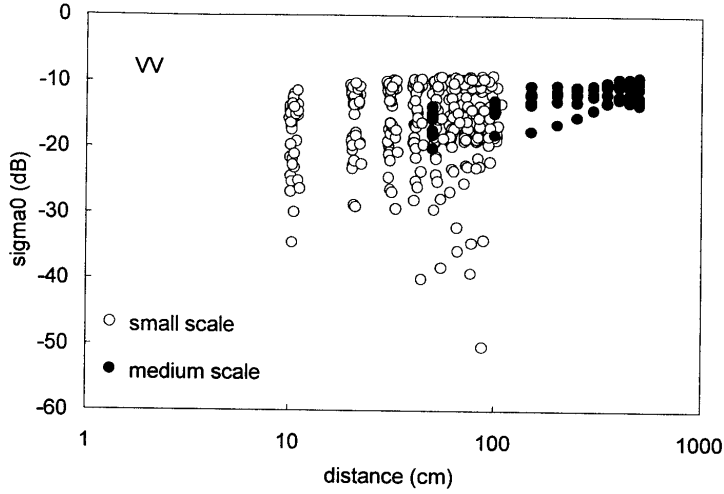

Figure 8. Surface backscattering coefficients calculated using ordinary one scale IEM and measured rms height and correlation length values of the many times deformed old ice field of Figure 4. All measurements have been carried out in the area of 100 m $\times$ 100 m. The distance is the radius of the area included in the calculations.

multiscale calculations maximum distances that produce the observed correlation length values (Fig. 3). It is natural that the difference between the single and multiscale results is smallest for the smoothest surfaces. The destructive effect of the multiscale exponential surface correlation of Eq. 13 extends up to larger distances, because it neglects a large part of the spherically symmetric surface correlation of Eq. 14. The isotropic exponential surface correlation is understandably more characteristic of natural surfaces than the mathematically more simple quadrangular exponential.

Usually increasing surface roughness leads to increasing backscattering. For example ice ridges are typically distinguished as curvilinear features of higher intensity values in SAR images. However, the many times deformed old ice area of Figure 9 presented one example of a long ridge indistinguishable in an ERS-1 SAR image, although the ridge was on average 1.1 m high and 4.2 m broad, which is at least the average size of ridges in the Baltic Sea [16]. Ridges of equal size

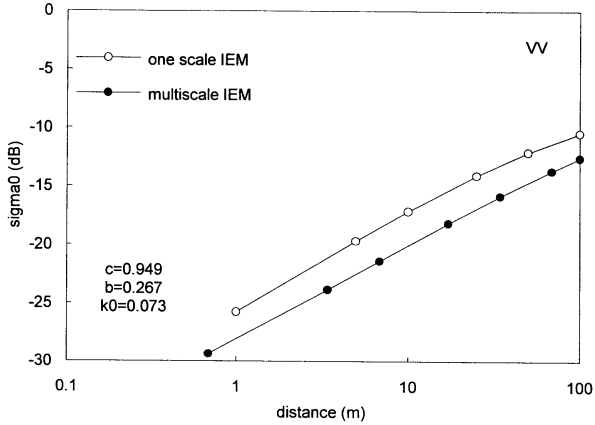

Figure 9. The surface backscattering coefficient of horizontal and vertical polarization calculated for the many times deformed old ice field where the medium scale roughness measurements were carried out in 1993 [15, 16, Fig. 8]. IEM has been applied to single scale or multiscale surface roughness with the isotropic exponential autocorrelation function. The distance is the radius of the area included in the backscattering calculations. The Kirchhoff and complementary field coefficients have been approximated with the radar incidence angle. The roughness parameter c corresponding to Eq. 7 is given using cm units for distance.

in the old ice area having a smoother background were detected in the same SAR image. The problem is not only that the average intensity of the deformed ice field was so high that it masked the ridges, but that the maximum intensity values really were smaller in the deformed area than in the smoother area. Since the sample areas are in the same SAR image, the effect can not be explained with calibration errors or the unfavourable incidence angle of ERS-1. Also, the ice of these two areas was equally old and originally similar. The temperature was well below zero during the satellite overpass and the snow cover was only partial. If the backscattering always increased with increasing surface roughness, the ridges in the deformed area should cause at least as high intensities as those of the ridged area. Thus it seems that some qualitative support for the possibility of a destructive effect of certain multiscale surface roughness exists.

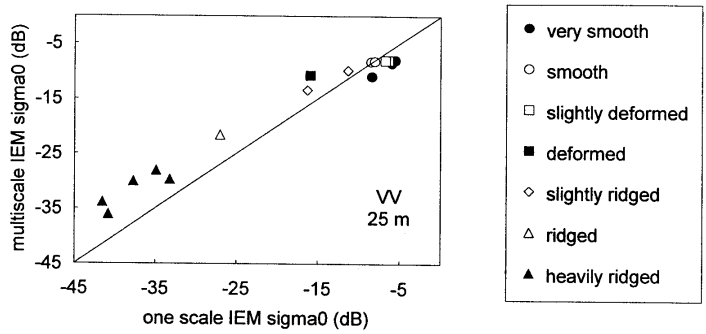

Figure 10. The surface backscattering coefficient of horizontal and vertical polarization calculated for various large scale ice types measured in 1994 [15, 16]. IEM has been applied to single scale or multiscale surface roughness with the isotropic exponential autocorrelation function. The Kirchhoff and complementary field coefficients have been approximated with the radar incidence angle. The calculations are made for an area with a radius of 25 m.

Although the qualitative behaviour of the multiscale surface roughness combined with the IEM is mostly acceptable, the quantitative results of the very rough ice types do not seem to be high enough. The multiscale treatment produces, at large distances, higher values than the ordinary IEM, but the backscattering level is still too low. The roughness of about the size of the wavelength used is reported to be the most important from the point of view of backscattering [3], but the smallest roughness scale does not dominate in Eqs. 2–5. However, it is well known that SAR images are also sensitive to the degree of large scale deformation of ice fields. Therefore, the larger roughness scales cannot be excluded when simulating the backscattering from sea ice. The problem of taking properly into account the large scale surface roughness is due to the limitations of validity of the Integral Equation Method as will be described in the following analysis.

The necessary condition for the rms slope to guarantee the validity of IEM is [4]

$$\frac{\sqrt{2\sigma}}{L} < 0.3 \tag{35}$$

where σ is the rms height and L the correlation length of the surface.

Another criterion for validity of IEM is required for dielectric surfaces when the local incidence angle of the Fresnel reflection coefficients is approximated with the radar incidence angle. For non-Gaussian surfaces the rule of thumb for validity is the following relationship for the surface and material parameters and frequency [3]

$$k^2\sigma L < 1.6\sqrt{\epsilon_r} \tag{36}$$

where k is the wave number and ϵ_r is the relative permittivity of the surface. Nevertheless, it is possible that IEM is valid even for larger values of σ and L. When the local incidence angle is approximated by specular angle the validity criteria of IEM replacing Eq. 36 is

$$kL > 5 \tag{37}$$

For surfaces of multiscale roughness, like Baltic sea ice, Eqs. 35 and 36 actually define the maximum and Eq. 37 the minimum dimension of the area (and roughness size) for which the IEM is guaranteed to be applicable. Combining them with Eqs. 6 and 7 we obtain

$$x < \left(\frac{0.3k_o}{\sqrt{2}c}\right)^{\frac{1}{b-1}} \tag{38}$$

$$x < \left(\frac{1.6\sqrt{\epsilon_r}}{k^2ck_o}\right)^{\frac{1}{b+1}} \tag{39}$$

$$x > \left(\frac{5}{kk_o}\right) \tag{40}$$

for Eqs. 35–37 respectively. For Baltic sea ice the local incidence angle condition is, in most cases, more restrictive than the rms slope condition. The maximum and minimum dimensions calculated for measured surfaces using Eqs. 38–40 are given in Table 1. The ERS-1 SAR frequency 5.3 GHz was used to calculate the wave number. The permittivity was taken to be 3.15, which is a common value for Baltic sea ice. It is obvious that neither of the two local incidence angle approximations alone permits the use of IEM for large areas, which are rough in all scales from small to large. In addition, in most cases there is a gap between the validity areas of these two approximations, so that even a piecewise approach using IEM is not possible.

	rms slope condition	local incidence angle condition	
surface type	maximum length of validity (m)	maximum length of validity (m)	minimum length of validity (m)
very smooth	0.34	2.90	4.45
very smooth	30.56	0.04	1.28
very smooth	10.58	0.04	1.58
smooth	15.63	0.80	2.58
smooth	2.86	0.09	1.89
slightly deformed	0.43	0.35	0.52
slightly deformed	0.39	0.25	0.41
deformed	1.55	0.10	4.69
slightly ridged	2.85	3.68	0.45
slightly ridged	0.99	0.90	0.38
ridged	37.70	0.03	1.24
heavily ridged	4.73	0.90	1.30
heavily ridged	3.47	0.66	1.93
heavily ridged	14.74	0.11	1.76
heavily ridged	31.46	0.09	0.88
heavily ridged	35.21	0.06	0.43

Table 1. The criteria (Eqs. 38 and 40) for the validity of IEM calculations for measured Baltic sea ice surfaces. The frequency used was 5.3 GHz, the radar incidence angle 23 ° and the permittivity 3.15.

The validity of IEM clearly varies quite remarkably for the surfaces measured. Still, it seems that in many cases IEM could be applied to areas comparable for example to the resolution of ERS-1 SAR, if the local incidence angle of the Fresnel reflection coefficients can be approximated with a better value than the radar incidence angle or zero.

The effect of the varying local incidence angle has been studied by calculating separately the Kirchhoff coefficients f_{pp} and the complementary field coefficients F_{pp} for all individual local incidence angles corresponding to two successive measured surface heights along the 50 m–100 m long surface roughness measurement lines [15]. The statistics of these parameters are given in Table 2. It is obvious that even a small variation of the local incidence angle may cause a large change in the values of the field coefficients. For horizontal polarization the field coefficients are monotonous and increase with increasing local incidence angle. For vertical polarization the effect of increasing the local incidence angle is more complicated and may increase or decrease the field coefficients.

	$\lvert f_{hh}\rvert^2$	$\lvert F_{hh}\rvert^2$	$\mathrm{Re}(f_{hh}^* F_{hh})$	$\lvert f_{vv}\rvert^2$	$\lvert F_{vv}\rvert^2$	$\mathrm{Re}(f_{vv}^* F_{vv})$
surface type	standard deviation/ average [%]	standard deviation/ average [%]	standard deviation/ average [%]	standard deviation/ average [%]	standard deviation/ average [%]	standard deviation/ average [%]
very smooth	2.9	18.3	-10.5	0.3	17.6	8.2
very smooth	2.9	18.2	-10.5	0.3	17.5	8.7
very smooth	1.4	8.6	-5.0	0.3	8.5	3.9
smooth	8.5	61.1	-30.8	1.3	56.5	22.5
smooth	11.2	82.4	-39.9	2.0	75.5	27.4
slightly deformed	10.5	92.7	-39.3	2.0	81.5	23.9
slightly deformed	12.9	97.8	-46.6	2.3	88.6	31.4
deformed	18.2	113	-62.0	3.4	105	44.2
slightly ridged	66.9	335	-193	13.4	297	70.9
slightly ridged	30.6	194	-101	6.4	176	58.6
ridged	108	389	-259	18.3	355	85.3
heavily ridged	564	678	-643	723	757	-917
heavily ridged	419	644	-570	399	685	-1274
heavily ridged	272	302	-292	310	314	-361
heavily ridged	114	262	-209	27.5	245	121
heavily ridged	796	796	0.0	831	806	7.2

Table 2. The ratio of standard deviation and average values of the terms $|f_{hh}|^2$, $|F_{hh}|^2$, $\mathrm{Re}\,(f_{hh}^* F_{hh})$, $|f_{vv}|^2$, $|F_{vv}|^2$, and $\mathrm{Re}\,(f_{vv}^* F_{vv})$ for measured surfaces of Baltic sea ice corresponding to Table 1.

Reliable determination of the Fresnel reflection coefficients for materials with low dielectric constant values is not easy, since the determination of the local incidence angle depends crucially on the chosen horizontal increment between the successive surface heights. The values used for Table 2 are rather moderate, since the distance was 50 cm. On the other hand, they represent the aerial statistics well, because the length of each line is 50–100 m. Similar analysis of small scale surface roughness measurements showed, that the average values of the local incidence angle, and thence also, the values of the terms involving field coefficients vary even more, when the statistics is calculated for intervals of 10 cm, 5 cm, 5 mm and 1 mm from the 1 m long measurement lines. In practice, it is not possible to measure very long distances with such small intervals. Therefore the results do not then represent a large area very reliably. The calculation of the field coefficients is a question that requires further investigation.

Although the backscattering level in Figures 9 and 10 is not reliable (Table 1, Eqs. 38 and 40), the general shape of the curve in Figure 9 is reasonable, if the ensemble average of the field coefficients does not vary strongly with changing distance. Moreover, the difference between the one scale and multiscale cases should not depend very strongly on the field coefficients.

5. DISCUSSION

The multiscale surface roughness description developed assumes the surfaces to contain all frequencies above a minimum value. For many natural surfaces having a long history, such as sea ice, this seems to be a good assumption. For more dynamic materials or targets consisting of several subtargets, the approach of separate frequency bands, also presented here, could be more promising. The same applies to cases, when the smallest scale of surface roughness has disappeared, like when the ice surface has melted and refrozen.

The radar return of a target depends on the backscattering integrated over individual pixels. The rms height, the autocorrelation function and average local incidence angle of an illuminated pixel characterize the pixel statistically from the point of view of backscattering. The rms height affects strongly the intensity level of the backscattering coefficient. The terms of the IEM backscattering coefficient involving the rms height of the surface decrease with increasing rms height for large values of σ [3]. Moreover, the spectrum for the surface correlation (Eqs. 31–34) increases with increasing correlation length. Therefore, without the field coefficients the net effect would typically be a decrease of the backscattering coefficient with an increase of the surface roughness. This is in contradiction with generally made observations of SAR images. Unfortunately, the field coefficients seem to have an important role in the surface backscattering calculations of materials of low permittivity. The reliable estimation of the magnitude of these parameters is though very difficult.

It is obvious that the approximation of the local incidence angle with the radar incidence angle (or zero angle) is not always well justified for very rough surfaces. This might explain the significant deviation of the calculated backscattering coefficient from the measured one, observed in some cases. It has often been suspected that this disagreement is a calibration problem of the measurements or due to a wrong value of the dielectric constant [4, 17]. Unfortunately this field coefficient approximation severely limits the validity of IEM for rough, low permittivity surfaces like Baltic sea ice (Table 1). This is evident also from the results of Figure 10, which show a systematic decrease in backscattering level with an increase of surface deformation. This is in contradiction with general observations. It seems that the high rms height values dominate the results, which are quite sensitive to the exact values of the surface roughness parameters. In conclusion, IEM is not yet

applicable to large pixels of very rough surfaces with low permittivity values like Baltic sea ice. Small laboratory samples with salinity resembling that of Arctic sea ice (which is roughly 10 times larger than that of Baltic sea ice) have been successfully modelled using IEM [12, 18]. The multiscale surface roughness of natural sea ice can be taken into account using the autocorrelation functions presented here, but further research of estimation of the field coefficients and of the effect of large rms height values is required.

The correlation length of surface heights relatively increases and the rms height decreases with increasing smoothness. In analogy, one may think that a large spatial correlation length of the backscattering coefficient combined with a small amplitude of its variation corresponds to a smooth surface, whereas a larger amplitude represents a rough surface. One might expect that for Baltic sea ice the interdependence of the backscattering coefficient rms height and correlation length is fractallike.

6. SUMMARY AND CONCLUSIONS

Autocorrelation functions describing surfaces with a continuous roughness spectrum were derived. A method to apply these functions to surfaces rough only in separate frequency bands is presented. Multiscale autocorrelation functions were found to approximate corresponding experimental curves of Baltic sea ice better than the ordinary single roughness scale autocorrelation functions. A multiscale surface description makes it easy to study the properties of a surface without having to fix in advance the exact wavelengths of interest.

Equations taking into account multiscale surface roughness, when calculating the surface backscattering coefficient, were developed. The results shown correspond to surfaces, where all individual roughness components have the same type of autocorrelation function and the same characteristic roughness parameters. The relationship between the roughness parameters and the distance is similar to that of fractallike surfaces. The results can easily be used to surfaces of piecewise homogeneous roughness characteristics. The method can also be applied to other types of surfaces with a continuous roughness range, if only the dependence of rms height and correlation length for the distance is known.

The problem of multiscale surface roughness, typical of natural surfaces like sea ice, can be taken into account by applying the method presented here, when modelling the backscattering using IEM. The problem that still requires further research is how to estimate the local incidence angles of the field coefficients. In the case of Baltic sea ice, it turned out that the determination of these parameters from measured surface heights is subject to large uncertainty. On the other hand, the use of the radar incidence angle instead of the local incidence angle severely limits the validity of IEM, when the target is rough and has a small dielectric constant. Because of the field coefficient approximation, IEM is mostly not suitable for large pixels of targets with multiscale surface roughness and small dielectric constant values like Baltic sea ice, although it seems to be applicable for smaller laboratory samples of artificial saline ice.

ACKNOWLEDGMENT

This study has been financially supported by the Finnish Board of Navigation and Technology Development Centre (TEKES).

REFERENCES

1. Church, E. L., "Fractal surface finish," *Applied Optics,* Vol. 27, No. 8, 1518–1526, 1988.
2. Keller, J. M., R. M. Crownover, and R. Y. Chen, "Characteristics of natural scenes related to the fractal dimension," *IEEE Trans. Pattern Anal. Machine Intell.,* Vol. PAMI-9, No. 5, 621–627, 1987.
3. Fung, A. K., *Microwave Scattering and Emission Models and Their Applications,* Artech House, Norwood, 1994.
4. Fung, A. K. and K. S. Chen, "Dependence of the surface backscattering coefficients on roughness, frequency and polarization states," *Int. J. Remote Sensing,* Vol. 13, No. 9, 1663–1680, 1992.
5. Fung, A. K., Z. Li, and K. S. Chen, "Backscattering from a randomly rough dielectric surface," *IEEE Trans. Geosci. Remote Sensing,* Vol. GE-30, No. 2, 356–369, 1992.
6. Ulaby, F. T., R. K. Moore, and A. K. Fung, *Microwave Remote Sensing,* Vol. II, Addison-Wesley, Reading, 1982.
7. Tsang, L., J. A. Kong, and R. T. Shin, *Theory of Microwave Remote Sensing,* John Wiley & Sons, New York, 1985.

8. Elson, J. M., J. P. Rahn, and J. M. Bennett, "Light scattering from multilayer optics: comparison of theory and experiment," *Applied Optics,* Vol. 19, No. 5, 669–679, 1980.
9. Elson, J. M., and J. M. Bennett, "Relation between the angular dependence of scattering and the statistical properties of optical surfaces," *J. Opt. Soc. Am.,* Vol. 69, No. 1, 31–47, 1979.
10. Lloyd, E. (ed.), *Handbook of Applicable Mathematics,* Vol. VI, Part B, John Wiley & Sons, Chichester, 1984.
11. Gradshteyn, I. S., and I. M. Ryzhik, *Table of Integrals, Series and Products,* Academic Press, New York, 1980.
12. Wolfram, S., *Mathematica, A System for Doing Mathematics by Computer,* Addison-Wesley, Redwood City, 1991.
13. Bredow, J. W., R. L. Porco, A. K. Fung, S. Tjuatja, K. C. Jezek, S. Gogineni, and A. Gow, "Determination of Volume and Surface Scattering from Saline Ice Using Ice Sheets with Precisely Controlled Roughness Parameters," *IEEE Transactions on Geoscience and Remote Sensing,* Vol. 33, No. 5, 1214–1221, 1995.
14. Churchhouse, R. F. (ed.), *Handbook of Applicable Mathematics, Vol III,* John Wiley & Sons, Chichester, 1981.
15. Manninen, A. T., "Surface roughness of Baltic sea ice," *Journal of Geophysical Research, Oceans,* in press.
16. Manninen, A. T., "Surface morphology and backscattering of ice ridge sails in the Baltic Sea," *Journal of Glaciology,* Vol. 42, No. 140, 141–156, 1996.
17. Evans, D. L., T. G. Farr, and J. J. van Zyl, "Estimates of surface roughness derived from synthetic aperture radar (SAR) data," *IEEE Trans. Geosci. Remote Sensing,* Vol. GE-30, No. 2, 382–389, 1992.
18. Beaven, S. G., G. L. Lockhart, S. P. Gogineni, A. R. Hosseinmostafa, K. Jezek, A. J. Gow, D. K. Perovich, A. K. Fung, and S. Tjuatja, "Laboratory measurements of radar backscatter from bare and snow-covered saline ice sheets," *Int. J. Remote Sensing,* Vol. 16, No. 5, 851–876, 1995.